biosensors

MDPI

Article

Viability of Neural Cells on 3D Printed Graphene Bioelectronics

Jingshuai Guo [1,†], Amir Ehsan Niaraki Asli [1,†], Kelli R. Williams [1], Pei Lun Lai [1], Xinwei Wang [1], Reza Montazami [1] and Nicole N. Hashemi [1,2,*]

[1] Department of Mechanical Engineering, Iowa State University, Ames, IA 50011, USA; jguo1@iastate.edu (J.G.); niaraki@iastate.edu (A.E.N.A.); kellij2@iastate.edu (K.R.W.); issaclun@iastate.edu (P.L.L.); xwang3@iastate.edu (X.W.); reza@iastate.edu (R.M.)

[2] Department of Biomedical Engineering, Iowa State University, Ames, IA 50011, USA

* Correspondence: nastaran@iastate.edu

† These Authors contributed equally to this work.

Received: 11 August 2019; Accepted: 17 September 2019; Published: 20 September 2019

Abstract: Parkinson's disease (PD) is the second most common neurodegenerative disease in the United States after Alzheimer's disease (AD). To help understand the electrophysiology of these diseases, N27 neuronal cells have been used as an in vitro model. In this study, a flexible graphene-based biosensor design is presented. Biocompatible graphene was manufactured using a liquid-phase exfoliation method and bovine serum albumin (BSA) for further exfoliation. Raman spectroscopy results indicated that the graphene produced was indeed few-layer graphene (FLG) with $(I_D/I_G)_{Graphene} = 0.11$. Inkjet printing of this few-layer graphene ink onto Kapton polyimide (PI) followed by characterization via scanning electron microscopy (SEM) showed an average width of ≈868 µm with a normal thickness of ≈5.20 µm. Neuronal cells were placed on a thermally annealed 3D printed graphene chip. A live–dead cell assay was performed to prove the biosensor biocompatibility. A cell viability of approximately 80% was observed over 96 h, which indicates that annealed graphene on Kapton PI substrate could be used as a neuronal cell biosensor. This research will help us move forward with the study of N27 cell electrophysiology and electrical signaling.

Keywords: Parkinson's Disease; mechanically exfoliated graphene; neuronal cells; electrical conductivity; biosensor

1. Introduction

Parkinson's disease (PD) is a neuronal disease that is caused by the death of dopaminergic neurons in the substantia nigra pars compacta region of the brain [1]. It is currently the second most common neurodegenerative disease in the United States after Alzheimer's disease (AD) [1,2]. Because of their dopaminergic properties [1], rat dopaminergic N27 cells have been widely used in in vitro models for PD studies [1,3]. They have also been used in studies seeking to understand problems such as neurotoxicity, oxidative stress, and histone deacetylase (HDAC) and other molecular pathways [4–6]. While there have been studies on synaptophysin signaling in N27 cells, the electrophysiological effects of graphene on N27 cells are currently unknown. Since a study on the electrophysiology of N27 cells is necessary to further understand PD and other neurodegenerative diseases, graphene may be helpful to better understand neurodegenerative diseases when employed as a biosensor.

Graphene is among the most widely used materials in the field of material science [7,8]. Graphene has a two-dimensional honeycomb nanostructure with a one-atom-thick planar sheet of sp^2-bonded carbon atoms [8–10]. Graphene has a large theoretical specific surface area of 2630 $m^2\ g^{-1}$ [11,12], intrinsic mobility of 200,000 $cm^2v^{-1}s^{-1}$ [13], and a superior thermal conductivity of approximately

5000 $Wm^{-1}K^{-1}$ [14]. Since it also has excellent electrical conductivity, it lends itself to many real-world applications and provides an ideal foundation for bioelectronics and biosensing [15,16].

Although there are currently many methods used to produce graphene, the end products are not biocompatible [17–19]. For example, popular graphene solutions such as dimethylformamide (DMF) and N-methylpyrrolidone (NMP) solutions are toxic and often result in low-concentration graphene solutions [20,21]. Therefore, it is necessary to develop a cell-friendly approach for large-scale production of biocompatible graphene. To address this problem, research was conducted on the synthesis of graphene-based solutions via oxidation and chemical vapor deposition (CVD) with the intent of improving these graphene fabrication methods [22–25]. However, there is evidence showing that the Hummer's method creates single carbon atom defects along with nano-sized cracks [26]. CVD works well for producing large, continuous films of graphene, but this method has been shown to result in numerous surface voids and defects [27], and its application has been only partly successful [28]. As the research of biocompatible graphene and its implementation in practical applications such as printing graphene have continued to grow, very few studies have been able to produce satisfying results [21]. Fortunately, the method of direct liquid-phase exfoliation (LPE) of graphite into graphene has been reported as an attractive approach for inkjet printing and cell-based studies.

There have been many previous studies on constructing biosensors using graphene-based materials [29]. One such example involved using graphene oxide (GO) to examine cellular DNA via the creation of graphene quantum dots (GQDs) [30]. The biosensors in another study primarily focused on the transfer of electrons and used CV to image cancer stem cells [31]. Also, while $[Fe(CN)_6]^{3-/4-}$ and $[Ru(NH_3)_6]^{3+/2+}$ redox peaks have been measured, a study on the bioelectrical signaling of neuronal cells using graphene-based sensors is lacking [30–33]. One advantage of using graphene in a biosensor study is that this material has no effect on mitochondrial membrane potential (MMP), mitochondrial morphology, or cell stress status [34]. Since graphene appears to have a bright future in biochemical and biomedical applications, engineers are encouraged to continue research studies on this material [34–37].

In this study, we describe a prototype graphene biosensor to sense electrical signaling in N27 cells. The biosensor was produced with an inkjet printer to create conductive, biocompatible, and defect-free graphene. The graphene was exfoliated from graphite using the LPE method. This design presents a facile technique that can be used to manufacture biosensors for a variety of applications. In a previous study, bovine serum albumin (BSA) was used to exfoliate graphene in an aqueous state and resulted in graphene that exhibited strong biocompatibility. Since this technique was easily implemented, it resulted suitable for large-scale graphene production and, hence, was adopted in this study. The graphene and printed graphene chips were characterized using Raman spectroscopy, Atomic force microscopy (AFM), and scanning electron microscopy (SEM). To characterize cell viability within the biosensor, multiple live–dead cell assays were performed.

2. Materials and Experimental Section

2.1. Materials and Equipment

The materials and equipment used in this study were: graphite (Synthetic powder, <20 µm, Sigma-Aldrich, St. Louis, MO, USA); Albumin, from bovine serum (bovine albumin* BSA, ≥98% agarose gel electrophoresis, lyophilized powder, Sigma-Aldrich, St. Louis, MO, USA); poly(sodium 4-styrenesulfonate) (PSS, Mw ~1,000,000 powder, Sigma-Aldrich, St. Louis, MO, USA); poly(ethyleneimine), (PEI) solution (50% *w*/*v*, Sigma-Aldrich, St. Louis, MO, USA); sodium chloride (NaCl) purchased from Sigma-Aldrich, St. Louis, MO, USA; Kapton polyimide (PI) (thickness: 0.008 mm, 100 × 100 mm, Sigma-Aldrich, St. Louis, MO, USA). RPMI medium 1640 (1X) (Ref#: 11875-093, 500 mL), L-glutamine 200 mM(100X) (Ref#: 25030-081, 100 mL), pen/strep solution (penicillin 10,000 U mL^{-1}/streptomycin 10,000 µg mL^{-1}, Ref#: 15140-122, 100 mL) was purchased from Gibco Life Technologies. Fetal bovine serum (FBS) (Qualified One Shot™, Ref#: A31606-01, 50 mL) was purchased from ThermoFisher Scientific, Waltham, MA. Polyurethane ether tubes (I.D.:0.063", Wall:0.031",

O.D.:0.125", Part Number: 2100070-100) were purchased from Superthane®, 3 mL Luer-Lok syringes were purchased from Allegro Medical. Inc. (Bolingbrook, IL, USA) Six-well cell culture clusters (Lot# 23314037) were purchased from Costar®. A GenieTouch™, syringe pump was purchased from Kent Scientific Corporation. A 4-axis CNC USB controller Mk3/4 for mini CNC mill was purchased and controlled by a PlanetCNC® (Ljubljana, Slovenia). A sinometer digital multimeter (MS8261) was used to measure print conductivity. A JEOL FESM JCM-6000 scanning electron microscope and a Zeiss Axio Observer Z1 inverted microscope were used for SEM imaging of the graphene prints and the live–dead cell assays, respectively. A Raman spectrometer (Voyage, B&W Tek, Inc., Newark, DE, USA) with a CW laser (Excelsior-532-150-CDRH, Spectra-Physics) was used for Raman spectroscopy measurements. A PerkinElmer UV–Vis spectrophotometer (Lambda 750) at λ = 660 nm at room temperature was used to provide absorption spectra and consequently the concentration of graphene ink.

2.2. Preparation of Graphene

The graphene solution used in this study was produced using the liquid exfoliation method. Wet-ball milling was used with both the Vibrio-Energy shaker mill [38] and a kitchen blender for further exfoliation [8]. The preparation of graphene, ink formulation and finally inkjet printing of the produced conductive ink is illustrated in Figure 1.The shear tension created by the steel balls helped further the exfoliation of graphene crystallites and led to the fabrication of high-quality FLG [38–40]. When using the Vibro-Energy (shaker) mill, 650 mg of graphite was mixed with 60 mg of BSA and was well dispersed in 35 mL of DI-H_2O. The Vibro-Energy mill (shaker mill) was run for 90 h at 300 rpm (Figure 1B). Twenty steel balls with a diameter of 8.7 mm (11/32") and 10 steel balls with a diameter of 4.5 mm (3/16") were added to all 5 containers (Figure 2A). A standard kitchen blender was run for 1 h at a speed of 16,761 rpm. Twenty grams of graphite was mixed with 605 mg of BSA well dispersed in 100 mL of DI-H_2O. Both graphene solutions were kept at rest for 24 h, allowing any remnant of non-dispersed graphite particles to sink to the bottom of the containers. Finally, in order to ensure repeatability of the formulated ink, the samples were collected from the top 80% of the solution, and the concentration of graphene was measured through UV–Vis spectroscopy. The resultant concentration resulted to be C $\approx$ 5.1 mg mL^{-1}.

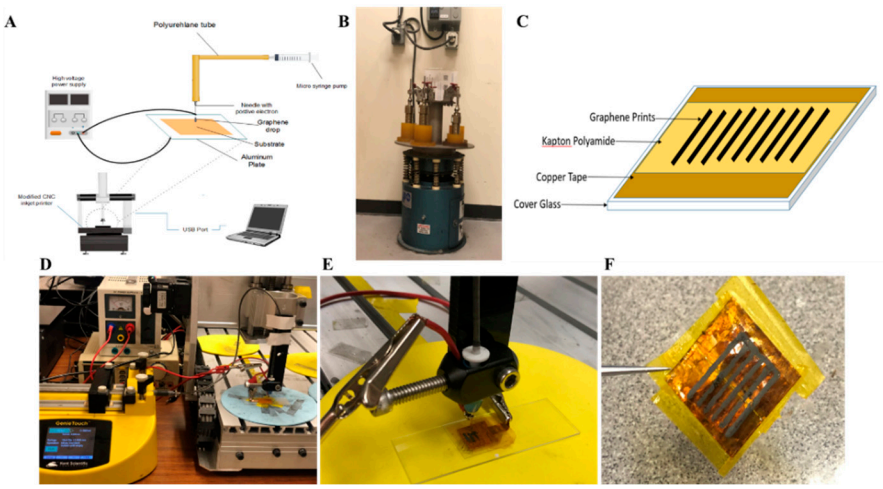

Figure 1. Schematic of the drop-on-demand graphene printing method. (**A**) An abridged general view of the printer setup. (**B**) A graphene solution was mixed using a Vibro-Energy mill (shaker mill) for 90 h at 300 rpm. (**C**) Schematic of chip setup. (**D**) Equipment setup during printing. A syringe pump was used along with an inkjet printer to deposit ink at a rate of 7 µL/s to ensure a constant flow rate throughout the syringe. (**E**) Needle and substrate setup. A 3 kV potential difference was introduced between the substrate and needle for the purpose of affixing ink onto the substrate. A cover glass was placed on a regular microscope slide for stability and support. (**F**). Printed chip end result of 3D printed graphene.

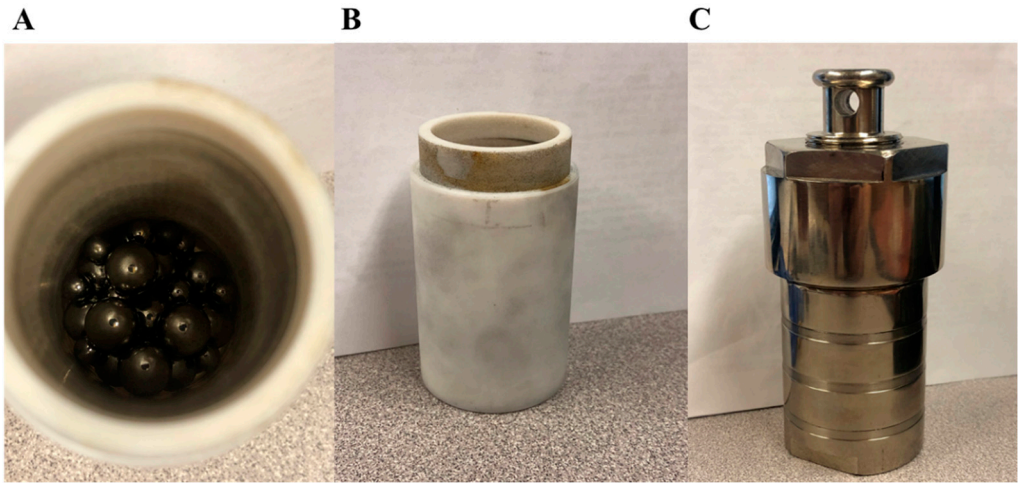

Figure 2. Graphene wet-ball milling container setup. (**A**) Twenty steel balls with a diameter of 8.7 mm (11/32″) and 10 steel balls with a diameter of 4.5 mm (3/16″) were added. (**B**,**C**) Container assembly for shaker mill.

2.3. Substrate Preparation

Because of its great thermal resistance, Kapton PI was chosen as the polymer substrate. It can withstand temperatures from −269 to 400 °C. Due to the hydrophilicity and negative charge of the FLG ink, it was necessary to perform a hydrophilicity treatment on the Kapton PI substrate. To treat Kapton PI, PI was first washed in acetone. The substrate was next washed with PSS (3.5 mg/mL), submerged in a solution of 50 mL DI-H_2O and NaCL (0.5 mol L^{-1}), and finally submerged into a PEI solution (30 mg/mL) of DI-H_2O and an NaCl solution (0.5 mol L^{-1}) for additional 20 min. The substrate was then allowed to air-dry for 12 h.

2.4. Inkjet Printing Procedure

The graphene ink was placed in a 5 mL syringe, and a 10 cm-long polyurethane ether tube was attached to this syringe. The graphene ink was injected through a hypodermic needle with an inner diameter of 300 µm. The syringe was fixed, and the graphene ink was injected via the syringe pump at a rate of 3 uL s^{-1}. The ink was injected onto the PI substrate, which was fixed on a 22 × 22 mm glass cover chip. The chip was covered with two pieces of copper tape, with a 0.50 mm gap between the two pieces (Figure 1C). A 3 kV potential difference was applied between the needle and the substrate, with the needle position being controlled by the CNC mini mill and its associated software. Prints were manufactured with a space of 800 µm between each print, and a total of five graphene lines were printed on one chip. Figure 1F shows the final printing result after annealing. A total of six graphene chips were made during each printing session.

2.5. Post-Processing and Conductivity Testing

Post-processing was performed for the purpose of improving the electrical conductivity and the stability of the printed graphene [41,42]. A set temperature of 280 °C was used to anneal the inkjet-printed graphene. After 30 min of annealing, the graphene chips were gently placed in a clear six-well plate. All chips required sterilization before introducing the cells. This allowed the cells to grow and increased the chances of their survival. A digital multimeter was used for conductivity testing, and the resistance of each line was measured every 3 mm across the gap created on the chip. The width of each line was then measured using a SEM and found to be 868 ± 20 µm; the height of each line measured by SEM was 4 ± 1 µm. The conductivity of each line could then be calculated from Equation (1), where R is the resistance of a printed line, l is its measured length, w is its width, and σ is the conductivity [43,44].

$$R = \frac{l}{wt\sigma} \quad (1)$$

Based on Equation (1), the conductivity measurements were performed by serval trails with different annealing temperatures and different time periods. Figure 3 shows the conductivity changes along annealing time and temperature change.

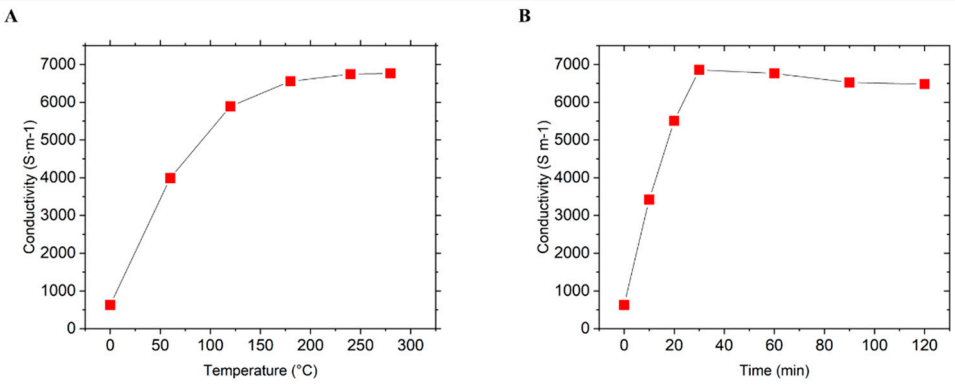

Figure 3. Conductivity measurements of printed graphene prints after treatment. (**A**) Conductivity changes dependent on the temperature, checked every 30 min. (**B**) Conductivity changes dependent on time at the same temperature of 280 °C.

2.6. Raman Spectroscopy

The samples obtained from the shaker mill and kitchen blender had similar cartelization when Raman spectroscopy was performed (Figure 4A). A thin film of graphene sample was prepared to determine the Raman spectra. A drop of the graphene sample with a diameter of approximately 10 mm was placed on top of a Si/SiO_2 substrate and air-dried. A Raman spectrometer with a CW laser provided a laser beam at wavelength 532 nm to the graphene on the Si/SiO_2 sample. Figure 4A depicts the Raman results for the graphene sample, on which five points were acquired by the Raman spectra. Figure 4B depicts the Raman results for the printed graphene lines on the Kapton substrate with comparisons of annealed graphene prints and non-annealed graphene prints.

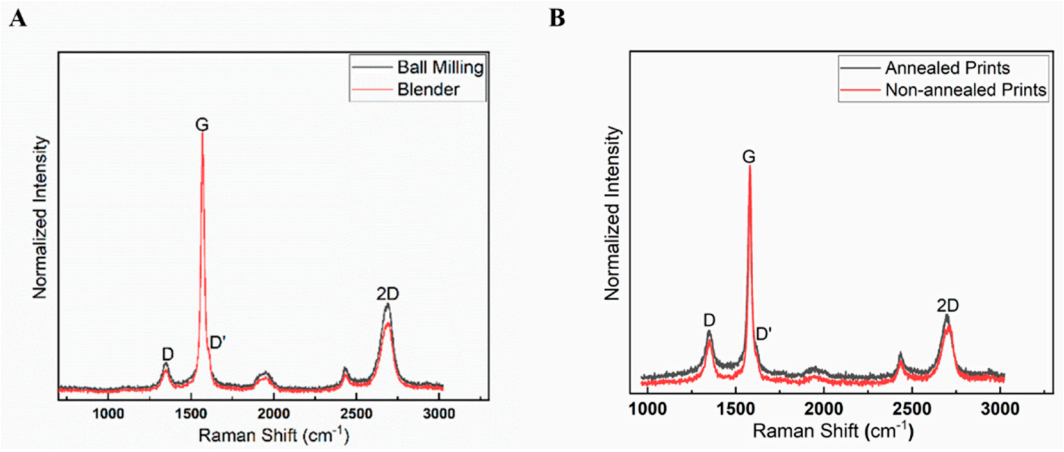

Figure 4. Raman spectra plot of both ball milling and blundered graphene under 532 nm laser. (**A**) Raman results for both ball milling and blender graphene samples on a Si/SiO_2 substrate. (**B**) Raman results for after annealed prints and non-annealed prints on Kapton tape.

2.7. Scanning Electron Microsopy and Atomic Force Microscopy

Imaging of the printed graphene patterns on PI was performed using a SEM with a 2–5 kV accelerating voltage. The thickness is shown in Figure 5 that displays images of prints after annealing.

AFM was applied to the graphene samples to characterize their thickness (Figure 6). A drop of graphene ink was positioned on a silicon slide and was dried on a warm plate in vacuumed chamber to ensure the precision of experiments.

2.8. Chip Biocompatibility Tests

A flask of eight-time-passaged N27 cells was chosen for testing the biocompatibility of the graphene sensor. The graphene chips were placed in six-well cell culture plates. The chips were then placed under a biological safety cabinet and exposed to UV radiation for 12 h. The UV exposure ensured that the chips were sterile and biocompatibility would be maximized. In this study, N27s cells were cultured in 3 mL of maintenance medium (MM) that included RPMI medium 1640 (1X), 10% FBS, 1% penicillin, and 1% L-glutamine. Then, 3 mL medium was introduced in each well which was covered with the graphene chip. N27 cells with a cell density $\geq 1 \times 10^6$ cells/vial were added to the chips using a micro pipette; 10 µL of cell suspension was introduced in each of the prints. The cells were left to grow in an incubator maintained at 37 °C with 5% CO_2. The cells were checked under an inverted microscope at 72 h, as shown in Figure 7.

2.9. Live–Dead Cell Assay

Live–dead cell assays were performed using a 70 µM CellTracker™ CMFDA solution combined with an 8 µM propidium iodide (PI) solution in FBS-free RPMI medium. The CellTracker™ CMFDA solution was prepared by dissolving 50 µg of CellTracker™ in 10.8 µL of dimethyl sulfoxide (DMSO). The PI was diluted from a stock provided by Invitrogen. The 70 µM CellTracker™ CMFDA solution and 80 µM PI solution were dissolved in FBS-free RPMI medium to reach the correct concentrations. Then, 1 mL of solution was prepared to facilitate the calculations and minimize the error. MM was carefully removed from the desired well of the 6-well plate. After removal, the well was rinsed with FBS-free RPMI medium (500 µL), 500 µL of dye was added to the well, and the cells were then incubated for 30 min at 37 °C in a 5% CO_2 atmosphere. The dye was then removed, and FBS-free RPMI medium was added to maintain moisture for sample imaging. N27 cells were imaged after 72 h of incubation. As shown in the control well (Figure 7A), live cells were colored in green, and dead cells were colored in red. Live and dead cells were also visible on the graphene chips. The chips were removed from the MM after incubation to ensure the cells were indeed growing on the chips and not on the well-plate surface, since the cells might have grown underneath the chips rather than on the chips. The chips were removed from the wells and transferred to clean wells with no MM.

A Zeiss Axio Observer Z1 inverted microscope was used to gather the live–dead cell assay results. The cells were carefully shielded from light after performing the live–dead cell assay so as to not affect the results. CellTracker™ CMFDA has an excitation of 492 nm and an emission of 517 nm. Propidium iodide has an excitation of 535 nm and an emission of 617 nm. The microscope was set to capture these wavelengths and image the fluorescence resulting from the live–dead cell assay. The results can be seen in Figure 7.

3. Results and Discussion

3.1. Chip Design

Traditional graphene-based biosensors are expensive and are still in a conceptual stage. One fabrication method consists in synthesizing graphene on a glass slip and etching SiO_2 with a Si/285 nm laser (34). Another fabrication method uses surface plasmon resonance to fabricate graphene on a gold sensor to achieve higher sensitivity than that of a traditional gold thin film SPR sensor [45].

In our design, the graphene biosensor chip included three components: a glass coverslip, a copper tape, and a polyimide (Kapton) polymer substrate (Figure 1). The copper tape was fixed on both sides of the chip with a 0.5 mm gap and fully covered by Kapton PI (Figure 1B) to prevent any

cellular exposure to copper. The chip may cause cytotoxic effects, and the goal was to minimize these effects [46]. Since the gap between the two pieces of copper tape was ≤0.5 mm, the Kapton PI substrate was used to connect the two pieces of tape with a flat surface. The effect of this gap on the 3D prints was negligible (Figure 1E) [47–49]. This design ensured that light could penetrate through the gap between the copper tape layers and reduced damage to the prints, offering an inexpensive physical method that is ready to use.

3.2. Printing Processes and Microscopy Studies

Aqueous graphene was pre-prepared using the wet-ball milling technology as described previously [50]. This paper focuses on graphene printing and sensor preparation. Graphene ink was applied to Kapton PI, using the custom-designed electronic inkjet printer represented in Figure 1. Because the FLG ink is hydrophilic and negatively charged [51], the PI substrate required some surface modification before successful printing could take place. The substrate was separately submerged into two different wetting agents, PSS and PEI, producing a hydrophilic layer on PI. This process created a hydrophilic buffer layer and changed the substrate from hydrophobic to hydrophilic [52]. A review of the literature disclosed that traditional inkjet printing uses a commercial printer that does not support high-viscosity ink. This negatively affects the print quality [24,53]. In this setup, graphene ink was directly injected using a needle and printed on a PI substrate. An electric field (Figure 1E) helped the ink fuse to the Kapton PI substrate. We found that printing at a flow rate of 3 µL/min, using a needle with an inner diameter of 300 µm and a 3 kV voltage, produced stable, continuous graphene prints with equal width and thickness (Figure 5A). The rather high value of the electric field was necessary to fix the conductive ink on the substrate [54].

To validate graphene quality, Raman spectroscopy of a graphene drop on SiO_2 was performed using a laser with a wavelength of 532 nm (Figure 4). A couple of key points can be taken from the Raman characterization. The acquired spectrum experienced a sharp G peak at ~1569.19 cm^{-1}, a symmetrical 2D peak at ~2689.55 cm^{-1}, and a D peak at ~1348.33 cm^{-1}, indicating that we had indeed achieved few-layer graphene [55]. Furthermore, the calculated $(I_D/I_G)_{Graphene}$ of the blender-mixed graphene was 0.11, while that of the wet-ball milled graphene was found to be 0.16. To further characterize the printed graphene, a SEM was used to produce SEM images (Figure 5) that confirmed that the graphene prints had an average width of 868 µm with no voids. This confirmed the purity of our graphene prints and that the graphene would be safe for biological use [56]. Additionally, The AFM results indicate a consistent thickness for the isolated graphene flake, which further confirms the Raman Spectra.

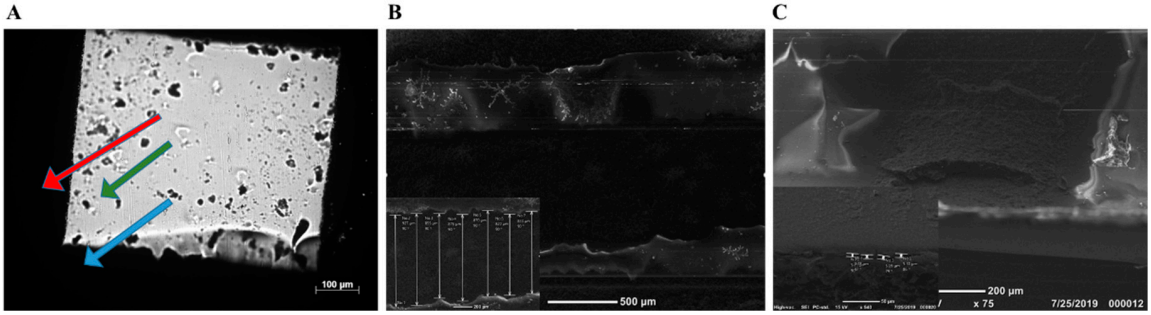

Figure 5. Microscope image of printing results. (**A**) An area of prints under the microscope. The red, blue, and green arrows indicate graphene, copper tape, and polyimide (PI), respectively, after the annealing process. (**B**,**C**) SEM images of printed graphene on PI using 2–5 kV accelerated voltage. (**B**) is a top-view image taken using SEM after annealing the prints with an average width of ≈868 µm. (**C**) shows an image of a cross section with an average depth of 5.20 µm.

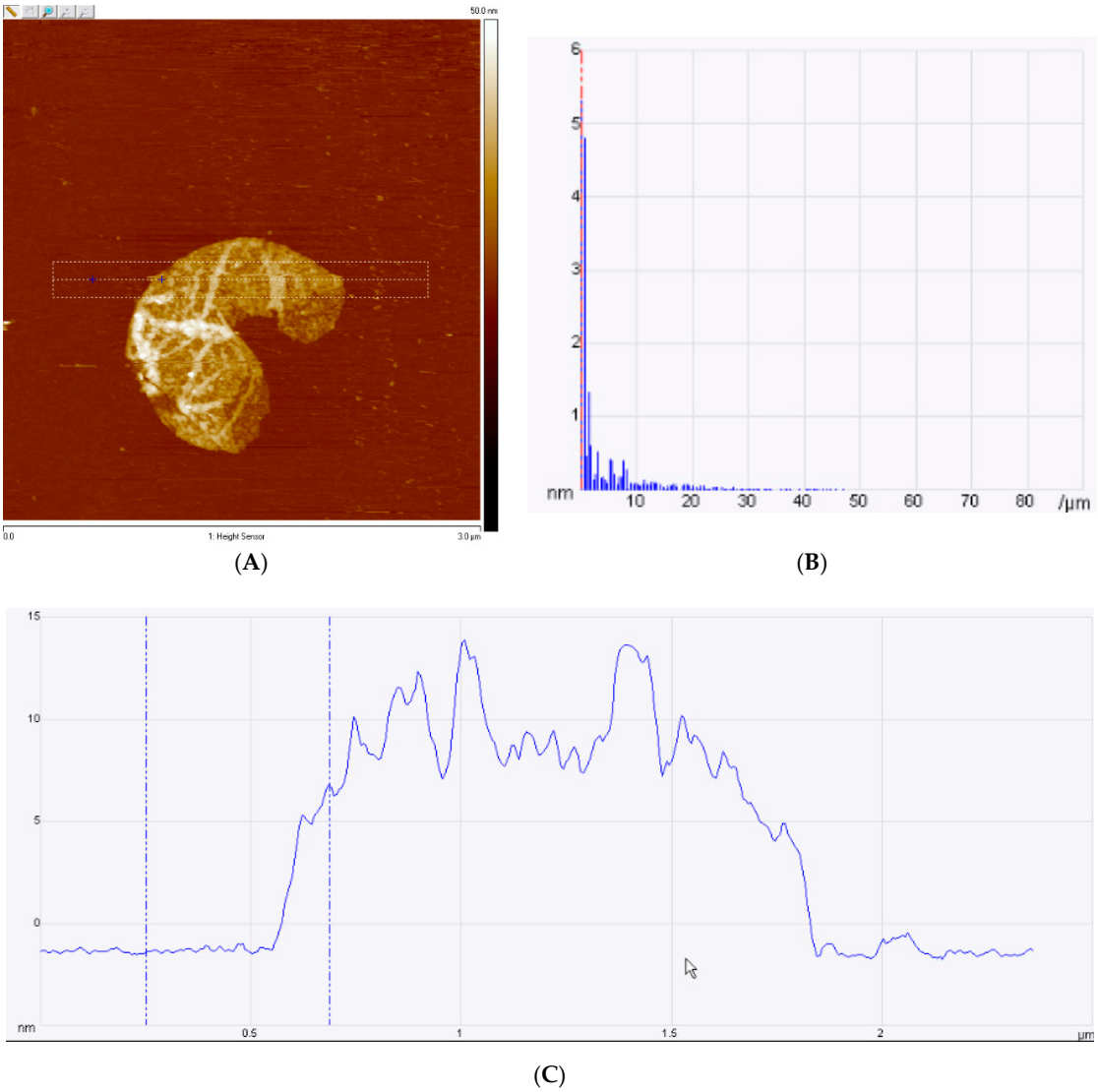

Figure 6. Atomic force microscopy (AFM) of graphene. (**A**) Graphene flake, (**B**) Spectral RMS amplitude was 5.33 nm. (**C**) AFM tapping frequency.

3.3. Post-Treatment of Graphene Prints

After undergoing the printing process, a thermal annealing process needed to be applied to complete the prints. This post-processing was necessary to prevent further disruption of the conductive network. The traditional solvents and surfactants used to perform graphite exfoliation can carry over into graphene production and may disrupt the conductive networks [21,44]. An oven was pre-heated to 280 °C to thermally treat the printed graphene. Graphene-printed chips were annealed for 30 min before being removed for conductivity measurements. Evidence shows that the properties of annealed graphene change as different annealing temperatures and times are applied [10,21,57–59]. The annealing process helps minimize FLG flake-to-substrate defects, improves print resistance, and cleans off any polymer contaminants still present on the graphene surface [60–62].

Multiple conductivity measurements were taken using a multimeter. Resistance of all five printed lines was measured across the gap for every 1 mm. From measuring the line resistance, a conductivity measurement approximately at 6800 $S \cdot m^{-1}$ was performed (Figure 3). By measuring in at different temperatures and different times, the changes in conductivity resulted negligible [63,64].

3.4. Biocompatibility Testing with N27 Cells

First, 3 mL RPMI medium was added into each well, and a 50 µL cell sample was added into the medium. N27 cells were observed under an inverted microscope after incubation for 24, 48, and 96 h. Figure 8 indicates the growth rate of the cells, demonstrating that after 72 h, the cells accounted for 85% of the live screen area. A live–dead cell assay was performed to confirm the survival rate of the cells grown on graphene [65,66]. It was expected that the cells would grow on top of the annealed Kapton and graphene. Polyimide materials are often used in biosensor research because of their strength and broad compatibility across research areas [67]. N27 cells fully expanded across the gap, connecting both sides of the graphene prints (Figure 7) [68,69]. From the live–dead cell assay results, it appeared that N27 cells successfully grew on the graphene and Kapton substrate, confirming our earlier hypothesis [69,70].

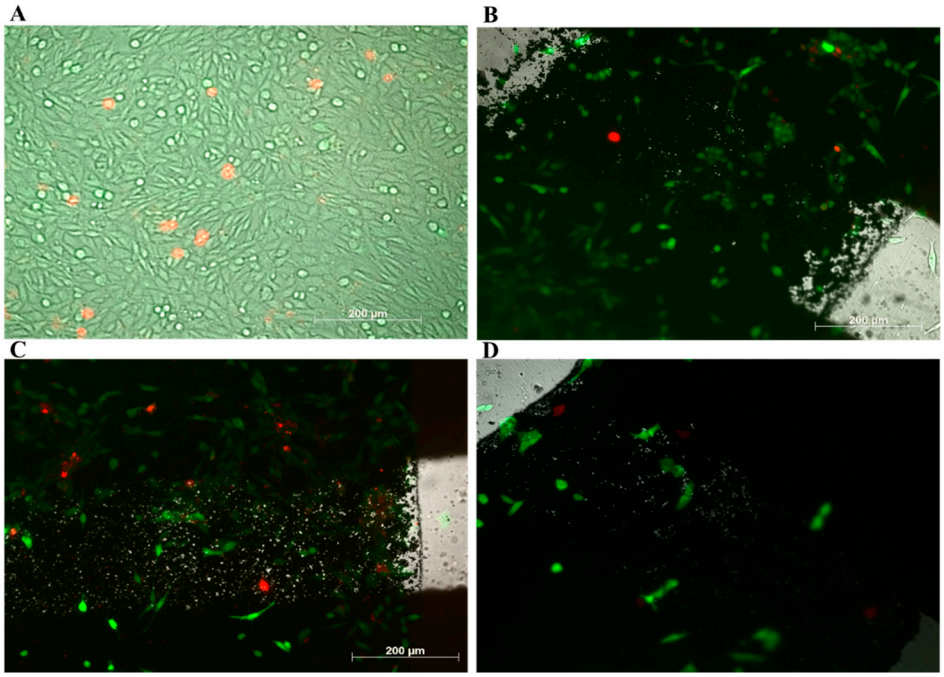

Figure 7. Cells cultured on graphene chips after 72 h of incubation. (**A**) Control well of N27 cells after 72 h at 37 °C in a 5% CO_2 atmosphere. (**B**–**D**) After 72 h of incubation, the cells expanded across a gap with a length of 290 µm.

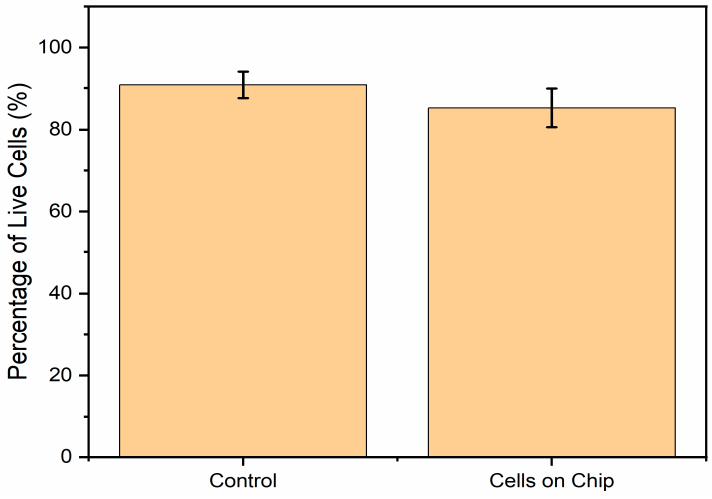

Figure 8. Percentage of live cells indicating that cell viability was approximately 85%.

It has been discussed in tissue-engineering literature that graphene may negatively affect the bimolecular mechanisms responsible for biological safety and toxicity [71–74]. Many reports have claimed that oxidative stress is one mechanism of cytotoxicity originating from carbon-based nanomaterials [75]. It is thought that graphene's sharp edges may cause cell membrane damage by physical interaction and lead to cytotoxicity [75–77]. Studies have also found evidence that graphene oxide is less toxic than graphene, while reduced graphene oxide and hydrogenated graphene solutions are much more toxic to neural cells. This may be due to the larger flake sizes present in these samples [72,78–81]. Such evidence provides support for our setup described above, in which there was no detectable cytotoxicity to the cells. Optical images also showed that only a small proportion of the cells were affected at the locations studied. These results could be beneficial for future N27 cell electrophysiology studies.

4. Conclusions

In conclusion, an easily applied and inexpensive biosensor design was presented characterized by a high percentage (85%) of live cells. This design could maximize printed FLG conductivity up to 6800 $S{\cdot}m^{-1}$ after thermal annealing. On the basis of live–dead cell assays result, it also proved to be biocompatible and not to interfere with cell adhesion and neuronal cell proliferation. This design proved that pristine graphene after thermal treatment does not have a harmful effect on neuronal cells. In addition, graphene printed on Kapton PI exhibited no detectable adverse effects on cell multiplication, mitochondrial morphology, or cell stress (34). This highlights a promising future for graphene, including long-term and stable biomedical applications, especially in bioelectrical studies on N27 cell electrophysiology.

Author Contributions: Conceptualization, J.G., A.E.N.A., K.R.W., P.L.L., R.M., N.N.H., and X.W.; methodology, J.G., A.E.N.A., K.R.W., P.L.L., R.M., N.N.H.; software, J.G., P.L.L., and A.E.N.A..; validation, J.G., K.R.W., and A.E.N.A.; formal analysis, J.G., and A.E.N.A.; investigation, J.G., K.R.W., A.E.N.A, P.L.L.; resources, N.N.H., R.M., and X.W.; data curation, J.G., A.E.N.A., K.R.W., and P.L.L.; writing—original draft preparation, J.G.; writing—review and editing, K.R.W., A.E.N.A, and N.N.H..; visualization, J.G. and A.E.N.A.; supervision, N.N.H., and R.M.; project administration, J.G.; funding acquisition, N.N.H., and R.M.

Funding: This work was partially supported by the Office of Naval Research Grant N000141712620 and the Iowa State University Department of Mechanical Engineering.

Acknowledgments: We thank Anumantha Kanthasamy of the Department of Biomedical Sciences at the Iowa State University for the gift of rat dopaminergic neural cells (N27s).

Conflicts of Interest: The authors declare no conflicts of interest.

References

1. Gao, L.; Zhou, W.; Symmes, B.; Freed, C.R. Re-Cloning the N27 Dopamine Cell Line to Improve a Cell Culture Model of Parkinson's Disease. *PLoS ONE* **2016**, *11*, e0160847. [CrossRef] [PubMed]
2. Poewe, W.; Seppi, K.; Tanner, C.M.; Halliday, G.M.; Brundin, P.; Volkmann, J.; Schrag, A.E.; Lang, A.E. Parkinson disease. *Nat. Rev. Dis. Primers* **2017**, *3*, 17013. [CrossRef] [PubMed]
3. Jagatha, B.; Mythri, R.B.; Vali, S.; Bharath, M.M. Curcumin treatment alleviates the effects of glutathione depletion in vitro and in vivo: Therapeutic implications for Parkinson's disease explained via in silico studies. *Free Radic. Biol. Med.* **2008**, *44*, 907–917. [CrossRef] [PubMed]
4. Harischandra, D.S.; Jin, H.; Anantharam, V.; Kanthasamy, A.; Kanthasamy, A.G. α-Synuclein Protects Against Manganese Neurotoxic Insult During the Early Stages of Exposure in a Dopaminergic Cell Model of Parkinson's Disease. *Toxicol. Sci.* **2015**, *143*, 454–468. [CrossRef]
5. Hammond, S.L.; Safe, S.; Tjalkens, R.B. A novel synthetic activator of Nurr1 induces dopaminergic gene expression and protects against 6-hydroxydopamine neurotoxicity in vitro. *Neurosci. Lett.* **2015**, *607*, 83–89. [CrossRef]
6. Wang, Y.; Wang, X.; Liu, L.; Wang, X. HDAC inhibitor trichostatin A-inhibited survival of dopaminergic neuronal cells. *Neurosci. Lett.* **2009**, *467*, 212–216. [CrossRef]

7. Geim, A.K.; Novoselov, K.S. The rise of graphene. In *Nanoscience and Technology*; Macmillan Publishers Ltd.: Lonodn, UK, 2009; pp. 11–19.
8. Pattammattel, A.; Kumar, C.V. Kitchen Chemistry 101: Multigram Production of High Quality Biographene in a Blender with Edible Proteins. *Adv. Funct. Mater.* **2015**, *25*, 7088–7098. [CrossRef]
9. Al-Sherbini, A.S.; Bakr, M.; Ghoneim, I.; Saad, M. Exfoliation of graphene sheets via high energy wet milling of graphite in 2-ethylhexanol and kerosene. *J. Adv. Res.* **2017**, *8*, 209–215. [CrossRef]
10. Gao, Y.; Shi, W.; Wang, W.; Leng, Y.; Zhao, Y. Inkjet printing patterns of highly conductive pristine graphene on flexible substrates. *Ind. Eng. Chem. Res.* **2014**, *53*, 16777–16784. [CrossRef]
11. Du, J.; Cheng, H.-M. The Fabrication, Properties, and Uses of Graphene/Polymer Composites. *Macromol. Chem. Phys.* **2012**, *213*, 1060–1077. [CrossRef]
12. Bolotin, K.I.; Sikes, K.J.; Jiang, Z.; Klima, M.; Fudenberg, G.; Hone, J.; Kim, P.; Stormer, H.L. Ultrahigh electron mobility in suspended graphene. *Solid State Commun.* **2008**, *146*, 351–355. [CrossRef]
13. Morozov, S.V.; Novoselov, K.S.; Katsnelson, M.I.; Schedin, F.; Elias, D.C.; Jaszczak, J.A.; Geim, A.K. Giant intrinsic carrier mobilities in graphene and its bilayer. *Phys. Rev. Lett.* **2008**, *100*, 11–14. [CrossRef] [PubMed]
14. Teweldebrhan, D.; Lau, C.N.; Ghosh, S.; Balandin, A.A.; Bao, W.; Calizo, I.; Teweldebrhan, D.; Miao, F.; Lau, C.N. Superior Thermal Conductivity of Single-Layer Graphene. *Nano Lett.* **2008**, *8*, 902–907.
15. Cai, W.; Zhu, Y.; Li, X.; Piner, R.D.; Ruoff, R.S. Large area few-layer graphene/graphite films as transparent thin conducting electrodes. *Appl. Phys. Lett.* **2009**, *95*, 2007–2010. [CrossRef]
16. Shao, Y.; Wang, J.; Wu, H.; Liu, J.; Aksay, I.A.; Lin, Y. Graphene based electrochemical sensors and biosensors: A review. *Electroanalysis* **2010**, *22*, 1027–1036. [CrossRef]
17. Cheng, J.-S.; Du, J.; Zhu, W. Facile synthesis of three-dimensional chitosan–graphene mesostructures for reactive black 5 removal. *Carbohydr. Polym.* **2012**, *88*, 61–67. [CrossRef]
18. Wang, L.; Wang, Y.; Xu, T.; Liao, H.; Yao, C.; Liu, Y.; Li, Z.; Chen, Z.; Pan, D.; Sun, L.; et al. Gram-Scale Synthesis of Single-Crystalline Graphene Quantum Dots with Superior Optical Properties. *Nat. Commun.* **2014**, *5*, 5357. [CrossRef] [PubMed]
19. Inamuddin, A.K.; Naushad, M. Optimization of glassy carbon electrode based graphene/ferritin/glucose oxidase bioanode for biofuel cell applications. *Int. J. Hydrogen Energy* **2014**, *39*, 7417–7421. [CrossRef]
20. Zhao, W.; Fang, M.; Wu, F.; Wu, H.; Wang, L.; Chen, G. Preparation of graphene by exfoliation of graphite using wet ball milling. *J. Mater. Chem.* **2010**, *20*, 5817–5819. [CrossRef]
21. Torrisi, F.; Hasan, T.; Wu, W.; Sun, Z.; Lombardo, A.; Kulmala, T.S.; Hsieh, G.W.; Jung, S.; Bonaccorso, F.; Paul, P.J. Inkjet-printed graphene electronics. *ACS Nano* **2012**, *6*, 2992–3006. [CrossRef]
22. Hummers, W.S.; Offeman, R.E. *Preparation of Graphitic Oxide*; ACS Publications: Washington, DC, USA, 1958.
23. Zhang, L.; Li, X.; Huang, Y.; Ma, Y.; Wan, X.; Chen, Y. Controlled synthesis of few-layered graphene sheets on a large scale using chemical exfoliation. *Carbon N. Y.* **2010**, *48*, 2367–2371. [CrossRef]
24. Huang, L.; Huang, Y.; Liang, J.; Wan, X.; Chen, Y. Graphene-based conducting inks for direct inkjet printing of flexible conductive patterns and their applications in electric circuits and chemical sensors. *Nano Res.* **2011**, *4*, 675–684. [CrossRef]
25. Liang, Y.T.; Hersam, M.C. Highly Concentrated Graphene Solutions via Polymer Enhanced Solvent Exfoliation and Iterative Solvent Exchange. *J. Am. Chem. Soc.* **2010**, *132*, 17661–17663. [CrossRef] [PubMed]
26. Dimiev, A.; Kosynkin, D.V.; Alemany, L.B.; Chaguine, P.; Tour, J.M. Pristine Graphite Oxide. *J. Am. Chem. Soc.* **2012**, *134*, 2815–2822. [CrossRef] [PubMed]
27. Suk, J.W.; Kitt, A.; Magnuson, C.W.; Hao, Y.; Ahmed, S.; An, J.; Swan, A.K.; Goldberg, B.B.; Ruoff, R.S. Transfer of CVD-Grown Monolayer Graphene onto Arbitrary Substrates. *ACS Nano* **2011**, *5*, 6916–6924. [CrossRef] [PubMed]
28. Kauling, A.P.; Seefeldt, A.T.; Pisoni, D.P.; Pradeep, R.C.; Bentini, R.; Oliveira, R.V.B.; Novoselov, K.S.; Castro Neto, A.H. The Worldwide Graphene Flake Production. *Adv. Mater.* **2018**, *30*, 1–6. [CrossRef]
29. Kuila, T.; Bose, S.; Khanra, P.; Mishra, A.K.; Kim, N.H.; Lee, J.H. Recent advances in graphene-based biosensors. *Biosens. Bioelectron.* **2011**, *26*, 4637–4648. [CrossRef]
30. Zhou, M.; Zhai, Y.; Dong, S. Electrochemical Sensing and Biosensing Platform Based on Chemically Reduced Graphene Oxide. *Anal. Chem.* **2009**, *81*, 5603–5613. [CrossRef] [PubMed]
31. Yang, S.; Guo, D.; Su, L.; Yu, P.; Li, D.; Ye, J.; Mao, L. A facile method for preparation of graphene film electrodes with tailor-made dimensions with Vaseline as the insulating binder. *Electrochem. Commun.* **2009**, *11*, 1912–1915. [CrossRef]

32. Lin, W.-J.; Liao, C.-S.; Jhang, J.-H.; Tsai, Y.-C. Graphene modified basal and edge plane pyrolytic graphite electrodes for electrocatalytic oxidation of hydrogen peroxide and β-nicotinamide adenine dinucleotide. *Electrochem. Commun.* **2009**, *11*, 2153–2156. [CrossRef]
33. Tang, L.; Wang, Y.; Li, Y.; Feng, H.; Lu, J.; Li, J. Preparation, Structure, and Electrochemical Properties of Reduced Graphene Sheet Films. *Adv. Funct. Mater.* **2009**, *19*, 2782–2789. [CrossRef]
34. Rastogi, S.K.; Raghavan, G.; Yang, G.; Cohen-Karni, T. Effect of Graphene on Nonneuronal and Neuronal Cell Viability and Stress. *Nano Lett.* **2017**, *17*, 3297–3301. [CrossRef] [PubMed]
35. Wang, R.; Shi, M.; Brewer, B.; Yang, L.; Zhang, Y.; Webb, D.J.; Li, D.; Xu, Y.Q. Ultrasensitive Graphene Optoelectronic Probes for Recording Electrical Activities of Individual Synapses. *Nano Lett.* **2018**, *18*, 5702–5708. [CrossRef] [PubMed]
36. Aziz, A.; Asif, M.; Azeem, M.; Ashraf, G.; Wang, Z.; Xiao, F.; Liu, H. Self-stacking of exfoliated charged nanosheets of LDHs and graphene as biosensor with real-time tracking of dopamine from live cells. *Anal. Chim. Acta* **2019**, *1047*, 197–207. [CrossRef] [PubMed]
37. Ryu, S.; Kim, B.S. Culture of neural cells and stem cells on graphene. *Tissue Eng. Regen. Med.* **2013**, *10*, 39–46. [CrossRef]
38. Thomas, D.-G.; Kavak, E.; Hashemi, N.; Montazami, R.; Hashemi, N. Synthesis of Graphene Nanosheets through Spontaneous Sodiation Process. *J. Carbon Res.* **2018**, *4*, 42. [CrossRef]
39. Yi, M.; Shen, Z. A review on mechanical exfoliation for the scalable production of graphene. *J. Mater. Chem. A* **2015**, *3*, 11700–11815. [CrossRef]
40. Sechi, D.; Greer, B.; Johnson, J.; Hashemi, N. Three-dimensional paper-based microfluidic device for assays of protein and glucose in urine. *Anal Chem.* **2013**, *85*, 10733–10747. [CrossRef]
41. Arapov, K.; Bex, G.; Hendriks, R.; Rubingh, E.; Abbel, R.; de With, G.; Friedrich, H. Conductivity Enhancement of Binder-Based Graphene Inks by Photonic Annealing and Subsequent Compression Rolling. *Adv. Eng. Mater.* **2016**, *18*, 1234–1239. [CrossRef]
42. Chen, H.; Müller, M.B.; Gilmore, K.J.; Wallace, G.G.; Li, D. Mechanically strong, electrically conductive, and biocompatible graphene paper. *Adv. Mater.* **2008**, *20*, 3557–3561. [CrossRef]
43. Das, S.R.; Nian, Q.; Cargill, A.A.; Hondred, J.A.; Ding, S.; Saei, M.; Cheng, G.J.; Claussen, J.C. 3D nanostructured inkjet printed graphene: Via UV-pulsed laser irradiation enables paper-based electronics and electrochemical devices. *Nanoscale* **2016**, *8*, 15870–15879. [CrossRef] [PubMed]
44. Secor, E.B.; Prabhumirashi, P.L.; Puntambekar, K.; Geier, M.L.; Hersam, M.C. Inkjet printing of high conductivity, flexible graphene patterns. *J. Phys. Chem. Lett.* **2013**, *4*, 1347–1351. [CrossRef] [PubMed]
45. Wu, L.; Chu, H.S.; Koh, W.S.; Li, E.P. Highly sensitive graphene biosensors based on surface plasmon resonance. *Opt. Express* **2010**, *18*, 14395. [CrossRef] [PubMed]
46. Studer, A.M.; Limbach, L.K.; Van Duc, L.; Krumeich, F.; Athanassiou, E.K.; Gerber, L.C.; Moch, H.; Stark, W.J. Nanoparticle cytotoxicity depends on intracellular solubility: Comparison of stabilized copper metal and degradable copper oxide nanoparticles. *Toxicol. Lett.* **2010**, *197*, 169–174. [CrossRef] [PubMed]
47. Caironi, M.; Gili, E.; Sakanoue, T.; Cheng, X.; Sirringhaus, H. High Yield, Single Droplet Electrode Arrays for Nanoscale Printed Electronics. *ACS Nano* **2010**, *4*, 1451–1456. [CrossRef] [PubMed]
48. Wang, S.; Ang, P.K.; Wang, Z.; Ling, A.; Tang, L.; Thong, J.T.L.; Loh, K.P. High Mobility, Printable, and Solution-Processed Graphene Electronics. *Nano Lett.* **2010**, *10*, 92–98. [CrossRef] [PubMed]
49. Xie, Y.; Yuan, P.; Wang, T.; Hashemi, N.; Wang, X. Switch on the high thermal conductivity of graphene paper. *Nanoscale* **2016**, *8*, 17581–17597. [CrossRef] [PubMed]
50. Aparna, R.; Sivakumar, N.; Balakrishnan, A.; Sreekumar Nair, A.; Nair, S.V.; Subramanian, K.R.V. An effective route to produce few-layer graphene using combinatorial ball milling and strong aqueous exfoliants. *J. Renew. Sustain. Energy* **2011**, *5*, 033123. [CrossRef]
51. Kim, Y.-K.; Min, D.-H. Durable Large-Area Thin Films of Graphene/Carbon Nanotube Double Layers as a Transparent Electrode. *Langmuir* **2009**, *25*, 11302–11306. [CrossRef] [PubMed]
52. Yoo, D.; Shiratori, S.S.; Rubner, M.F. Controlling bilayer composition and surface wettability of sequentially adsorbed multilayers of weak polyelectrolytes. *Macromolecules* **1998**, *31*, 4309–4318. [CrossRef]
53. Nur, H.M.; Song, J.H.; Evans, J.R.G.; Edirisinghe, M.J. Ink-jet printing of gold conductive tracks. *J. Mater. Sci. Mater. Electron.* **2002**, *13*, 213–219. [CrossRef]
54. Yudistira, H.T.; Nguyen, V.D.; Dutta, P.; Byun, D. Flight Behavior of Charged Droplets in Electrohydrodynamic Inkjet Printing. *Appl. Phys. Lett.* **2010**. [CrossRef]

55. Saito, R.; Hofmann, M.; Dresselhaus, G.; Jorio, A.; Dresselhaus, M.S. Raman spectroscopy of graphene and carbon nanotubes. *Adv. Phys.* **2011**, *60*, 413–550. [CrossRef]
56. Sanchez, V.C.; Jachak, A.; Hurt, R.H.; Kane, A.B. Biological Interactions of Graphene-Family Nanomaterials: An Interdisciplinary Review. *Chem. Res. Toxicol.* **2012**, *25*, 15–34. [CrossRef] [PubMed]
57. Majee, S.; Liu, C.; Wu, B.; Zhang, S.L.; Zhang, Z.B. Ink-jet printed highly conductive pristine graphene patterns achieved with water-based ink and aqueous doping processing. *Carbon N. Y.* **2017**, *114*, 77–83. [CrossRef]
58. Overgaard, M.H.; Kühnel, M.; Hvidsten, R.; Petersen, S.V.; Vosch, T.; Nørgaard, K.; Laursen, B.W. Highly Conductive Semitransparent Graphene Circuits Screen-Printed from Water-Based Graphene Oxide Ink. *Adv. Mater. Technol.* **2017**, *2*, 1–7. [CrossRef]
59. Tan, R.K.L.; Reeves, S.P.; Hashemi, N.; Thomas, D.G.; Kavak, E.; Montazami, R.; Hashemi, N.N. Graphene as a flexible electrode: Review of fabrication approaches. *J. Mater. Chem. A* **2017**, *5*, 17777–17803. [CrossRef]
60. Vasilieva, F.D.; Kapitonov, A.N.; Yakimchuk, E.A.; Smagulova, S.A.; Antonova, I.V.; Kotin, I.A. Mildly oxidized graphene oxide suspension for printing technologies. *Mater. Res. Express* **2018**, *5*, 65608. [CrossRef]
61. Lin, Y.-C.; Lu, C.-C.; Yeh, C.-H.; Jin, C.; Suenaga, K.; Chiu, P.-W. Graphene Annealing: How Clean Can It Be? *Nano Lett.* **2011**, *12*, 414–419. [CrossRef]
62. Xie, Y.; Xu, Z.; Xu, S.; Cheng, Z.; Hashemi, N.; Deng, C.; Wang, X. The defect level and ideal thermal conductivity of graphene uncovered by residual thermal reffusivity at the 0 K limit. *Nanoscale* **2015**, *7*, 10101–10110. [CrossRef]
63. Xu, F.; Ge, B.; Chen, J.; Nathan, A.; Xin, L.L.; Ma, H.; Min, H.; Zhu, C.; Xia, W.; Li, Z.; et al. Scalable shear-exfoliation of high-quality phosphorene nanoflakes with reliable electrochemical cycleability in nano batteries. *2D Mater.* **2016**, *3*, 025005. [CrossRef]
64. Hernandez, Y.; Nicolosi, V.; Lotya, M.; Blighe, F.M.; Sun, Z.; De, S.; McGovern, I.T.; Holland, B.; Byrne, M.; Gun'Ko, Y.K.; et al. High-yield production of graphene by liquid-phase exfoliation of graphite. *Nat. Nanotechnol.* **2008**, *3*, 563–568. [CrossRef] [PubMed]
65. Pemathilaka, R.L.; Caplin, J.D.; Aykar, S.S.; Montazami, R.; Hashemi, N.N. Placenta-on-a-Chip: Placenta-on-a-Chip: In Vitro Study of Caffeine Transport across Placental Barrier Using Liquid Chromatography Mass Spectrometry (Global Challenges 3/2019). *Glob. Chall.* **2019**, *3*, 1800112. [CrossRef]
66. Hashemi, N.; Lackore, J.M.; Sharifi, F.; Goodrich, P.J.; Winchell, M.L.; Hashemi, N. A paper-based microbial fuel cell operating under continuous flow condition. *Technology* **2016**, *4*, 98–103. [CrossRef]
67. Sun, Y.; Lacour, S.P.; Brooks, R.A.; Rushton, N.; Fawcett, J.; Cameron, R.E. Assessment of the biocompatibility of photosensitive polyimide for implantable medical device use. *J. Biomed. Mater. Res. Part A* **2009**, *90A*, 648–655. [CrossRef] [PubMed]
68. Bai, Z.; Mendoza Reyes, J.M.; Montazami, R.; Hashemi, N. On-chip development of hydrogel microfibers from round to square/ribbon shape. *J. Mater. Chem. A* **2014**, *2*, 4878–4884. [CrossRef]
69. McNamara, M.C.; Sharifi, F.; Okuzono, J.; Montazami, R.; Hashemi, N.N. Microfluidic Manufacturing of Alginate Fibers with Encapsulated Astrocyte Cells. *ACS Appl. Bio Mater.* **2019**, *2*, 1603–1613. [CrossRef]
70. Acar, H.; Çinar, S.; Thunga, M.; Kessler, M.R.; Hashemi, N.; Montazami, R. Study of physically transient insulating materials as a potential platform for transient electronics and bioelectronics. *Adv. Funct. Mater.* **2014**, *24*, 4135–4143. [CrossRef]
71. Ruiz, O.N.; Fernando, K.S.; Wang, B.; Brown, N.A.; Luo, P.G.; McNamara, N.D.; Vangsness, M.; Sun, Y.P.; Bunker, C.E. Graphene oxide: A nonspecific enhancer of cellular growth. *ACS Nano* **2011**, *5*, 8100–8107. [CrossRef]
72. Bramini, M.; Alberini, G.; Colombo, E.; Chiacchiaretta, M.; DiFrancesco, M.L.; Maya-Vetencourt, J.F.; Maragliano, L.; Benfenati, F.; Cesca, F. Interfacing Graphene-Based Materials with Neural Cells. *Front. Syst. Neurosci.* **2018**, *12*, 12. [CrossRef]
73. Caplin, J.D.; Granados, N.G.; James, M.R.; Montazami, R.; Hashemi, N. Microfluidic Organ-on-a-Chip Technology for Advancement of Drug Development and Toxicology. *Adv. Healthc. Mater.* **2015**, *4*, 1426–1450. [CrossRef] [PubMed]
74. Sharifi, F.; Patel, B.B.; Dzuilko, A.K.; Montazami, R.; Sakaguchi, D.S.; Hashemi, N. Polycaprolactone Microfibrous Scaffolds to Navigate Neural Stem Cells. *Biomacromolecules* **2016**, *17*, 3287–3297. [CrossRef] [PubMed]

75. Seabra, A.B.; Paula, A.J.; De Lima, R.; Alves, O.L.; Durán, N.D. Nanotoxicity of Graphene and Graphene Oxide. *Chem. Res. Toxicol.* **2014**, *27*, 159–168. [CrossRef] [PubMed]
76. Akhavan, O.; Ghaderi, E. Toxicity of Graphene and Graphene Oxide Nanowalls Against Bacteria. *ACS Nano* **2010**, *4*, 5731–5736. [CrossRef] [PubMed]
77. Hu, W.; Peng, C.; Luo, W.; Lv, M.; Li, X.; Li, D.; Huang, Q.; Fan, C. Graphene-Based Antibacterial Paper. *ACS Nano* **2010**, *4*, 4317–4323. [CrossRef] [PubMed]
78. Donaldson, K.; Aitken, R.; Tran, L.; Stone, V.; Duffin, R.; Forrest, G.; Alexander, A. Carbon Nanotubes: A Review of Their Properties in Relation to Pulmonary Toxicology and Workplace Safety. *Toxicol. Sci.* **2006**, *92*, 5–22. [CrossRef] [PubMed]
79. Akhavan, O.; Ghaderi, E.; Akhavan, A. Size-dependent genotoxicity of graphene nanoplatelets in human stem cells. *Biomaterials* **2012**, *33*, 8017–8025. [CrossRef]
80. Ou, L.; Song, B.; Liang, H.; Liu, J.; Feng, X.; Deng, B.; Sun, T.; Shao, L. Toxicity of graphene-family nanoparticles: A general review of the origins and mechanisms. *Part Fibre Toxicol.* **2016**, *13*, 57. [CrossRef]
81. Kurapati, R.; Backes, C.; Ménard-Moyon, C.; Coleman, J.N.; Bianco, A. White Graphene undergoes Peroxidase Degradation. *Angew. Chem. Int. Ed.* **2016**, *55*, 5506–5511. [CrossRef]